Silicon nanoparticle loaded CaV_4O_9 microflowers for robust high capacity Li-ion Battery anodes

A thesis

submitted in partial fulfilment of the requirements for the

BS-MS Dual Degree Programme

by

Minal Wable

(20141177)

Under the guidance of

Prof. Satichchandra B Ogale

IISER PUNE

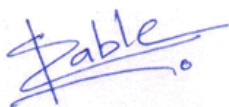**Indian Institute of Science Education and Research, Pune**

Dr. Homi Bhabha Road,

Pashan, Pune 411008, INDIA.

April, 2019

Certificate

This is to certify that this dissertation entitled " **Silicon nanoparticle loaded CaV₄O₉ microflowers for robust high capacity Li-ion Battery anodes**" towards the partial fulfilment of the BS-MS dual degree programme at the Indian Institute of Science Education and Research, Pune represents study carried out by **Minal Wable** at Indian Institute of Science Education and Research under the supervision of **Prof. Satishchandra B Ogale**, Professor, Department of Physics, during the academic year 2018-2019.

Minal Wable

Registration Number: 20141177

Prof. Satishchandra B Ogale

Supervisor

Committee:

Prof Satishchandra B Ogale (Supervisor)
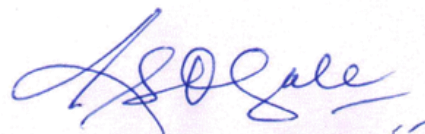
Dr. Partha Hazra (TAC)

Declaration

I hereby declare that the matter embodied in the report entitled " **Silicon nanoparticle loaded CaV$_4$O$_9$ microflowers for robust high capacity Li-ion Battery anodes**" are the results of the work carried out by me at the Department of Physics, Indian Institute of Science Education and Research, Pune, under the supervision of **Prof. Satishchandra B Ogale** and the same has not been submitted elsewhere for any other degree.

· Minal Wable

Registration number: 20141177

Prof. Satishchandra Ogale

Supervisor

This thesis is dedicated to my parents……

Acknowledgement

I would like to express my heartfelt gratitude and respect for my supervisor Prof. Satishchandra Ogale for the continuous support during the thesis study and related research. His guidance helped me in at time to overcome difficulties and finish my project. His strong motivation and immense knowledge has always directed me well during my research period. I understand that these words are not enough to acknowledge, but still I would like to express my grartitude towards him. I am also grateful to my fellow labmates for their co-operation, for providing me a lively lab atmosphere for working and for the stimulating lab meetings. I must take a special mention of the immense help by Dr. Reshma, Dr. Neha and Dr. Subas.

I thank Mr. Yathish and Mr. Anil Prathamshetti who helped me in obtaining the FESEM data and also, Mr. Prashant for helping me in acquiring the TEM data. I am thankful to Department of Science and Technology (DST), for the financial support by providing me INSPIRE fellowship. I am also thankful to the Infosys Foundation Endowment Fund for providing me the financial support during my undergraduate studies. I am grateful to Department of Physics and Chemistry at IISER Pune, all teaching and non-teaching staff, who have helped me directly and indirectly and finally IISER Pune for providing an excellent academic atmosphere.

I would like to express my profound gratitude towards my family, for their immense love and continuous encouragement throughout all these years, which has helped me to come so far and achieve everything till this phase of education. Last but not the least, I am obliged to all my dear friends especially Gaurav, Swathi, Abhijit, Sarah, Sravya and Ashwini who accepted nothing less than fineness in me and have been a constant help and support.

Minal Wable

Table of Contents

Table of figures

Abbreviations

BET – Brunauer–Emmett–Teller

CMC – Carboxymethyl Cellulose

CV – Cyclic Voltammetry

CVO – Calcium vanadium oxide

DFEC – Di-fluoro ethylene carbonate

DFT – Density Functional Theory

DMC – Dimethyl carbonate

EC – Ethylene carbonate

EDX – Energy Dispersive X-ray Analysis

EIS – Electrochemical impedance spectroscopy

FEC – Fluoro ethylene carbonate

FESEM – Field Emission Scanning Electron Microscopy

FWHM – Full width at half maximum

IR – Infra red

LIB – Lithium-ion battery

LCO – Lithium cobalt oxide

NMP – N-Methyl-2-pyrrolidone

PC – Propylene carbonate

SEI – Solid electrolyte interface

Si-NPs – Silicon nanoparticles

XRD – X-ray Diffraction

Abstract

Lithium-ion batteries are being constantly investigated so to enhance their properties like high energy density, rate performance and cycling stability. Calcium Vanadium Oxide (CVO) has been explored in this context since vanadium has the multi-electron transfer property which leads to higher stable capacity. Calcium oxide nanograins formed during a redox reaction buffers the volume change of electrodes. Silicon is another interesting option for anode material which provides higher capacity but within a few cycles, the capacity fades away, as it undergoes very high volume expansion and contraction in the discharge/charge cycles. The present study demonstrates that a physical mixture of CaV_4O_9 microflowers and Si nanoparticles (Si-NPs) synergistically acts to enhance the capacity as well as stability of the anode based upon such a mixture.

The CaV_4O_9 microflowers were first synthesized by using the hydrothermal synthesis method. The prepared samples were characterized by scanning electron microscopy, powder X-ray diffraction and transmission electron microscopy. Anodes based upon CaV_4O_9, silicon nanoparticles (Si-NPs) and the CaV_4O_9/Si-NPs composites were then prepared and tested for their capacity and cycling stability. The Li-ion storage performance in pristine materials and the composites were analysed by Galvanostatic charge-discharge measurements, at a current density of 1 A g^{-1}. The pristine CVO exhibits a stable specific capacity of 90 mAh g^{-1}, the Si-NPs exhibit very high initial discharge capacity of 2398 mAh g^{-1}, but it degrades after mere 50 cycles. The CVO-Si-NPs (80-20) composite shows a stable specific capacity of 450 mAh g^{-1}, and the CVO-Si-NPs (50-50) composite shows very high and a stable specific capacity of 800 mAh g^{-1} up to 100 cycles, proving that the composite can be utilised as an efficient anode in Li ion battery.

Chapter 1

INTRODUCTION

To create a sustainable society, we need to move towards sustainable energy resources, leaving behind the practice of non-renewable energy sources like coal, oil and natural gas. The use of these energy sources leads to CO_2 emissions, global warming and other adverse effects on humankind and other species[1]. Renewable energy resources such as solar energy and wind energy offer a solution to these problems but can't be utilised to the fullest because of their intermittency. This is where energy harvesting and storage play a vital role to ensure uninterrupted energy availability. Therefore, energy storage systems have gained significant attention and especially batteries due to its high energy density, rate performance, cycling stability, safety and its application in convenient electronic devices and electric vehicles. The energy and power distribution of various energy storage devices is shown in Figure 1.1, and it can be seen that lithium-ion batteries are of great importance as power sources to satisfy the ever-increasing energy demands.
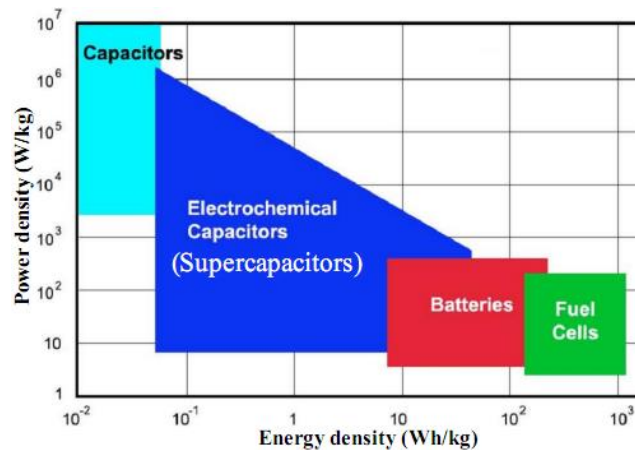
Figure 1.1: Ragone plot for comparison of various energy-storage devices[2]

1.1   Charge storage devices

A charge storage device is an apparatus used to store energy and release it whenever needed. The charge storage happens by oxidation and reduction reactions that take place on electrodes. Charge storage can be done in two ways; surface storage and bulk storage. Surface storage includes supercapacitor where the charge storage takes place without undergoing redox reactions. Bulk storage includes batteries where redox reactions take place on electrodes to store the charge.

Batteries are classified based on their life cycle; primary batteries function till the active elements are used up, and once the reactants are consumed they cannot be recharged. While secondary batteries are the rechargeable batteries that allow energy to restore in the cell and can be used several times. In these batteries, the chemical reactions can be reversed by applying an external potential.

1.2 Historical development in batteries

Batteries carry an old history with first battery invented in 1749 and since then they are under constant development and improvisation. In 1749, Benjamin Franklin first coined the term "battery" to explain a set of linked capacitors used for experiments with electricity[3]. In 1800, Alessandro Volta invented first true battery where he piled pair of copper and zinc discs one after other[4]. In 1836, John F. Daniell developed the most improved version of voltaic cell known as Daniell cell[5]. Since then, the battery has been the most widespread source of electricity. In 1859, Gaston Plante invented a first rechargeable battery that was recharged by altering the current and is known as a lead-acid battery[6]. Later on, nickel cadmium and the nickel iron-based batteries were invented[7, 8]. By 1990, nickel-based batteries were gaining attention in the market due to their good capacity, power density, cost and better environmental tolerance. In 1970, Stan Whittingham discovered a way to diffuse Li-ion in titanium sulfide sheets[9] and in 1980, an American chemist; John B Goodenough developed first LIB where he used Li_xCoO_2 as the cathode which is a more stable and lighter oxide[10]. In 1991, Sony Corporation licensed $LiCoO_2$ as a cathode material and used graphite as anode and LIBs were commercialized. It was then followed by Li-ion polymer batteries in 1991 and nano-phosphate LIBs in 2001[9].

Li-ion batteries have been a topic of research since then and have been used in a wide variety of applications from small wearable devices to grid storage. The research in Li-ion batteries is directed towards enhancing the power and energy density of the device to meet the energy demands and eliminate fossil fuel usage[11].

1.3 The Working principle of Lithium-ion battery

During charging, the external voltage is applied across the battery due to which the Li-ions present in the cathode (+) move through the electrolyte towards the anode (-) and similarly, electrons move from cathode to anode, but through an external circuit. During discharging, an external load is applied, the stored Li-ions move back

towards cathode through electrolyte and electron flow from anode to the cathode through the outer circuit. When all the ions have moved back, the battery gets fully discharged. The working principle is shown in Figure 1.2.
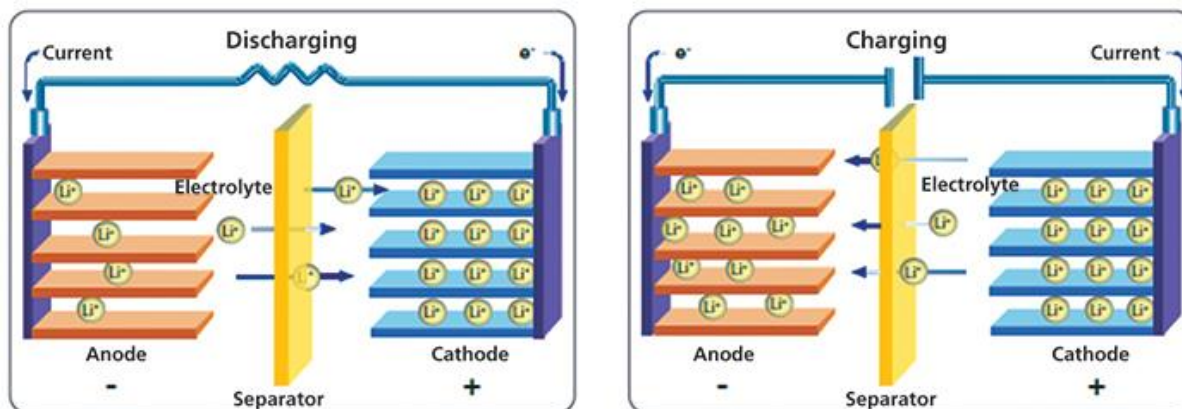
Figure 1.2: Graphic demonstration for working of Li-ion battery[12]

1.4 Components of battery

1.4.1 Cathodes

A cathode is the positive electrode in the battery and usually a 3d transition metal ion containing compound. The cathodes are of different types namely layered, spinel, olivine and tavorite depending on the crystal structure and atom arrangement.

The various cathodes used in Li ion battery are:

1.4.1.1 Transition metal oxide

The layered transition metal oxides have been used as cathodes since lithium cobalt oxide (LCO) is being used as a commercialized electrode by Sony[13, 14]. LCO is very good cathode material with a theoretical capacity of 274 mAh g^{-1}, high stability and high operating voltage 4.2 V. The concerns associated with cathodes are the thermal instability, rapid capacity fading at high rates[15, 16]. Lithium nickel oxide (LNO) is other explored cathode material and with an advantage of relatively lower cost of nickel the cobalt.

1.4.1.2 Polyanionic compounds

Polyanionic compounds are a popular class of cathode materials, generally $(XO_4)^{3-}$ where X-(Si, S, P, Mo) comprising compounds with polyanions occupying lattice positions. These compounds increase the cathode working potential of cathodes

which leads to an increase in power density. For example, $LiFePO_4$ has an olivine structure with good thermal stability and high power density[17].

1.4.2 Anodes

Batteries are composed of various elements and anode, the negative electrode in the battery, being one of the major constituents determines the life and stability of a battery. In batteries, anode material should have a high gravimetric capacity and high cycling stability even at high active material loading to realize them as commercial batteries. To achieve this, the following requirements should be satisfied by anode: 1) volume change during charging-discharging should be less so that the structure is stable and creates small mechanical stress; 2) good electrochemical reversibility and a high gravimetric capacity; 3) tapping density of active material should be high, which will decrease the electrode's thickness and effectively decrease the distance that charge will travel; 4) ion diffusion kinetics and electric conductivity kinetics should be high for efficient transport of ions and electrons[18].

Among all alkali metal, lithium is the lightest metal with a very high specific capacity of 3800 mAh g^{-1}, and thus, it can be used as an anode material with high energy density. But, the dendrite formation of Li metal during high C-rate leads to the shortening of a cell. Also, it's unsafe to use Li metal as it catches fire when it comes in contact with the moisture. So, anodes other than Li metal are essential, and they are classified into various types depending on their Li storage mechanism. Figure 1.3 shows the schematic representation of Li storage in different ways.

1.4.2.1 Intercalation anodes

In this case, the anode material store Li-ions by intercalation without undergoing any chemical reactions and it is stored by Coulombic and Van der Waals interactions. Graphite is a highly popular intercalation anode material in LIBs. The interlayer distance between the two planes of graphene is suitable for the Li-ions as the size of the ion matches with the interlayer distance. It stores 1 Li atom per 6 carbon atoms and its theoretical capacity is 372 mAh g^{-1} [19]. The first LIBs were made using graphite anode and LCO cathode but were not suitable for high energy density battery application[20].
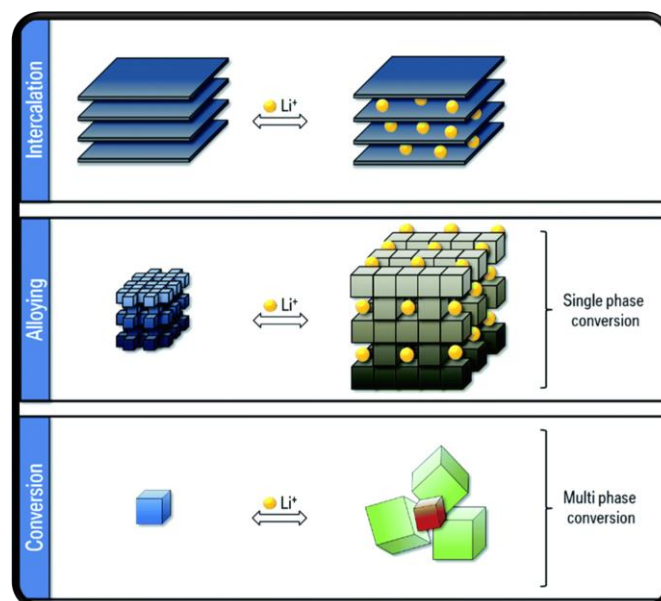
Figure 1.3: Schematic illustration of various types of anode materials [21]

1.4.2.2   Alloying anodes

For alloying anodes, reactive metals like Si, Sn, Al, Mg, Ag, Sb, etc. form an alloy with Li metal. These are promising anode material for LIBs due to high energy capacity and higher power density. The theoretical capacity of alloying anodes is several times higher than graphite. These anodes with Al and Si have potential onset value of 0.3-0.4 V above Li/Li$^+$ which ensures no plating of lithium at extremely low potentials. Unlike graphite, the alloying anodes can accommodate many of lithium ions which leads to higher volume expansion, and the electrode undergoes cracking and pulverisation causing capacity decay[22].

1.4.2.3   Conversion anodes

Here, the conversion-metal undergoes displacement reactions with lithium during the cycling. This material is being explored as possible best anodes for future alkali-ion batteries. Mostly transition metal is coupled with alloying elements where the transition metal undergoes a change from ionic state to its metallic state, and the alloying element takes part in the cycling process[23]. When transition metal sulfides are used as conversion materials, upon incorporation of Li-ion they are expected to form Li_2S nano-composites and metal. These materials show a high capacity of around 600 mAh g^{-1}.

1.4.3 Separators

The separator is a porous film placed between positive and negative electrodes. Separators prevent the electrical contact between anode and cathode and thus avoid the shortening of the cell. The separator which is a semipermeable membrane that selectively passes ions but not electrons and therefore it is ionically conducting and electronically insulating. The pore size of the separator should be compatible with the ion size, and it should be thermally stable and chemically inactive[24]. The generally used separator is Whatman, which is made of cellulose and is a good conductor of Na and Li ions. Other that Whatman, polypropylene based separators are also used in battery which is called as Celgard that are used for materials with high volume expansion like Silicon.

1.4.4 Binders

A binder plays an important role in an electrochemical performance of Li-ion batteries. It is used in the process of making an electrode. It acts as an active mixing agent to unite the electrode species together and then steadily adhere them to the current collectors[25]. Polyvinylidene fluoride (PVDF) is the commonly used binder, but carboxymethyl cellulose (CMC) binder remarkably improves the cycling stability, rate performance of anode and proper adhesion to the current collector.

1.4.5 Electrolytes and additives

An electrolyte serves the purpose of ion transport medium between the electrodes. The liquid electrolyte has to solvate the Li-ion as they come out of the electrode and these solvated ions have to move back and forth between the electrodes. It also has to desolate, so that Li-ion can enter the opposite electrode. In Li-ion battery, electrolytes generally have Li salt dissolved in carbonate, ether, ester or an ionic liquid solvent. Lithium hexafluorophosphate ($LiPF_6$) in ethylene carbonate (EC) and dimethyl carbonate (DMC) is the commercial electrolyte used in Li-ion battery. Electrolytes should be stable over a wide temperature range, have a large potential window of operation, low viscosity and high dissolution for Li salts, and should be cheap, non-toxic and environmentally friendly[26].

Additives are added so that the solid electrolyte layer (SEI) layer is stable and then there is no irreversible capacity loss in further cycles. Fluoroethylene carbonate (FEC) is commonly used additives which forms a stable SEI layer.

1.5   Vanadium based anode materials

In the past couple of years, various reports have demonstrated calcium based nanostructures such as calcium sulfate nanowires, calcium germinate nanowires, calcium vanadate nanowires and calcium silicate nanowires which exhibit potential application in the fields of optical devices, electronic devices and electrochemical sensors[27]. Among ternary metal vanadates, calcium vanadate shows a budding application in LIBs due to its electrochemical and lithium insertion properties[28]. In the present study, the focus will be calcium vanadium oxide since the calcium ions are electrochemically inactive and forms calcium oxide nano-grains which buffers the volume change of the electrodes. In addition to this, vanadium is abundant and inexpensive, and also its multiple oxidation states which results in multi-electron transfer can improve the performance of battery[29]. Due to strong V-O bond strength, the valence of vanadium cannot reach zero at low voltage, and thus vanadium oxides possess potentially smaller volume change when used as an anode material. The binary oxides of vanadium like V_2O_5, V_2O_3 limits the efficiency of the battery as it exhibits poor electrical conductivity and poor reaction kinetics[30].Thus, unlike the typical conversion reaction based anodes, CVO satisfies the essential properties of the electrode material[18].

1.6   Silicon

Silicon (Si) is the second most abundant element on the earth, and its exceptional ability to form an alloy with lithium leads to a high specific capacity. The theoretical capacity of silicon is 4200 mAh g^{-1} as each silicon atom can incorporate 4.4 Li atoms[31]. But, the silicon-based anode undergoes huge volume expansion (~300%) during charging which leads to the cracking and de-lamination of material on the electrode during discharging[32, 17]. This leads to a rapid capacity decrease and prevents this material from getting commercialised. Si nanostructures like nanowires, nanotubes etc. have been proposed to mitigate this problem because the smaller particles reduce the overall size of Li-Si alloy minimising volume expansion[33, 34]. Apart from this, Si composites with robust materials such as carbon have been proposed where the material act as a buffer to the volume expansion and prevents the pulverisation. The efforts are currently directed towards developing a composite which is easy to synthesize, possessing required properties, and involving eco-friendly methods and compounds[35]. Therefore, herein we prepared a composite of

Si-NPs with CaV_4O_9 (CVO) microflowers by physical mixing in various ratios and tested these as anode materials for Li-ion battery. The composite is seen to have a better performance than pristine materials which is validated by the obtained results.

Chapter 2

Experimental techniques

2.1 Materials and methods

2.1.1 Chemicals and materials

Glycerol ($C_3H_8O_3$), Calcium Hydroxide ($Ca(OH)_2$), Vanadium Pentoxide (V_2O_5), 30%-Hydrogen Peroxide (H_2O_2),Silicon nanoparticles (Si-NPs) Conducting carbon, NMP, Ethylene Carbonate(EC), Dimethyl Carbonate(DMF), Lithium hexafluorophosphate ($LiPF_6$), Celgard 2300 membrane, Lithium metal and Copper foil.

2.1.2 Synthesis of CaV$_4$O$_9$ micro-flowers

For the synthesis of CaV$_4$O$_9$ micro-flower, 10 ml of Glycerol was added to 10 ml water and stirred for 30 min. Later, 1 mmol of $Ca(OH)_2$ was added to it to make solution- A. Along with this, 2 mmol of V_2O_5 was dissolved in 10 ml DI water and stirred for 30 min, and then 8 ml H_2O_2 (30%) was added dropwise to form solution-B (carried out in the absence of light). Both the solution was stirred for 1 h and then mixed, and the final solution was stirred for 2.5 h. It was then was transferred to a 50 ml Teflon-lined container, and inserted in stainless steel autoclave. The autoclave was hydrothermally treated at 200° for 48 h, and was cooled down to room temperature. The resultant dark blue powder was washed a few times with DI water and ethanol and then dried at 70°C for 24 h.

2.1.3 Hydrothermal Methods

Hydrothermal growth of crystal was first reported by Karl Emil von Schafhäult in 1845 where he used a pressure cooker to grow microscopic quartz crystals. Hydrothermal method is used to synthesize nanocrystals in water conditions under high temperature and pressure for the substances which are insoluble in ordinary conditions. It is used to prepare good quality crystals, and due to rough reaction condition, the reaction rate is increased to almost 3-fold. Usually, for such synthesis, the reaction mixture is kept in a Teflon lined container, and this is then inserted in stainless steel autoclave and packed tightly with screws and treated at high temperature. Crystal size and shape of the materials obtained after synthesis

depends on the solvent, precursor and temperature for the reaction. The density of solvent and dielectric constant are also important parameters that affect the solvating ability. The materials that are not stable at their melting point can also be grown using this technique. And, this technique can be coupled with microwave, ultrasound, mechanochemistry and hot pressing to increase the reaction kinetics.

Teflon liner   Stainless steel autoclave

Figure 2.3.1 Images of the hydrothermal autoclave with Teflon liner vessel

2.2   Analysis Techniques

2.2.1 X-ray diffraction (XRD)

It is a non-destructive and rapid method that is used for the determination of atomic and molecular structure of a crystal. It gives the details of lattice parameters, crystal size and anisotropic growth involved in materials. X-rays are the form of electromagnetic radiation that lies in the wavelength range of 0.01nm to 10nm. The wavelength of X-ray and the inter-planar distance between the atoms of crystal are the same in order of magnitude and hence can be used for determination of crystal.

When a monochromatic beam of X-rays is incident on the sample, they are diffracted to different direction based on the electron cloud density within the crystal structure. The diffracted beams of X-ray undergo constructive and destructive interference that add up and cancel each other during respective processes. The condition for constructive interference is given by Bragg's law (Figure 2.3.2 (a)):

$$2d \sin \theta = n\lambda$$

Where d- inter-planar distance

Θ- Angle of scattering

n- Order of diffraction

λ- Wavelength of an incident X-ray beam.

PXRD was carried out using Bruker D8-Advance X-ray Diffractometer (Germany) with Cu kα (wavelength – 1.5418 Å) (Figure 2.3.2 (b)).
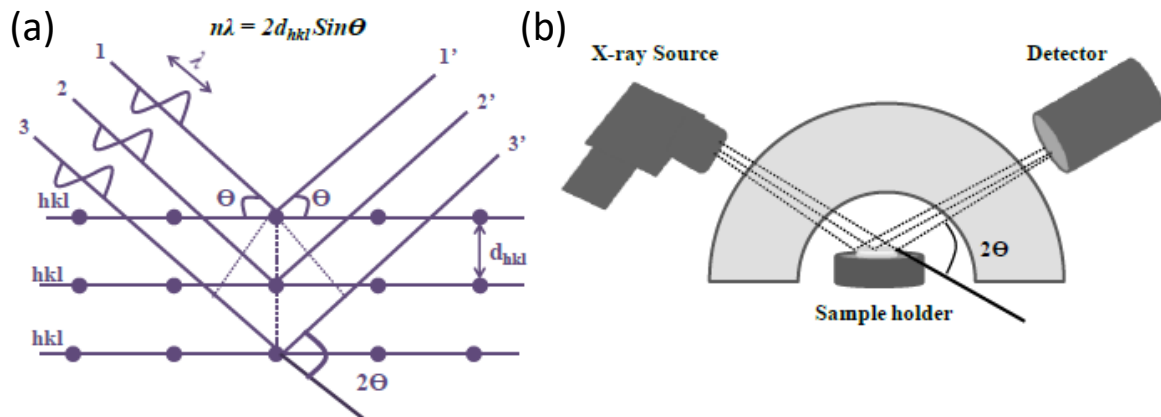

Figure 2.3.2: Schematic for illustration of (a) Bragg's Diffraction (b) Bruker D8 Advance X-ray Diffractometer

2.2.2 Field Emission-Scanning Electron Microscopy (FESEM)

FESEM is used to visualize tiny topographic minutiae on the entire surface of the sample. An electron gun placed at the top of the microscope produces an intense primary electron beam by field emission source which is accelerated in high electric field gradient and directed towards the sample (Figure 2.3.3). Field emission gun is more reliable in terms of cleaner image, fewer electron distortions and spatial resolution less than 2nm. The bombardment of these primary electrons on the sample produces secondary electrons. The detector collects these secondary electrons and processes the signal to obtain a high-quality image. The detector is kept at high vacuum around 10^{-7} torr so that the loss of electron is prevented[26]. The resolution of the microscope is limited by aberration or diffraction which has a different origin. The lower limit of diffraction for spatial resolution in optical microscopy is around 200nm while for an electron beam of E= 5 KeV, λ can be calculated by de Broglie's wavelength.

$$\text{de Broglie's wavelength,} \ \lambda = \frac{h}{\sqrt{2mE}}$$

11

where h- Plank's constant

m- Mass of electron

E- Kinetic energy of an electron

Therefore, the spatial resolution of an electron microscope is higher than a conventional optical microscope, and the limit for resolution in electron microscope turns out to be 0.017 nm. Scanning electron microscopy (SEM) was done using FEI Nova Nano 450 SEM (Figure 2.3.3).
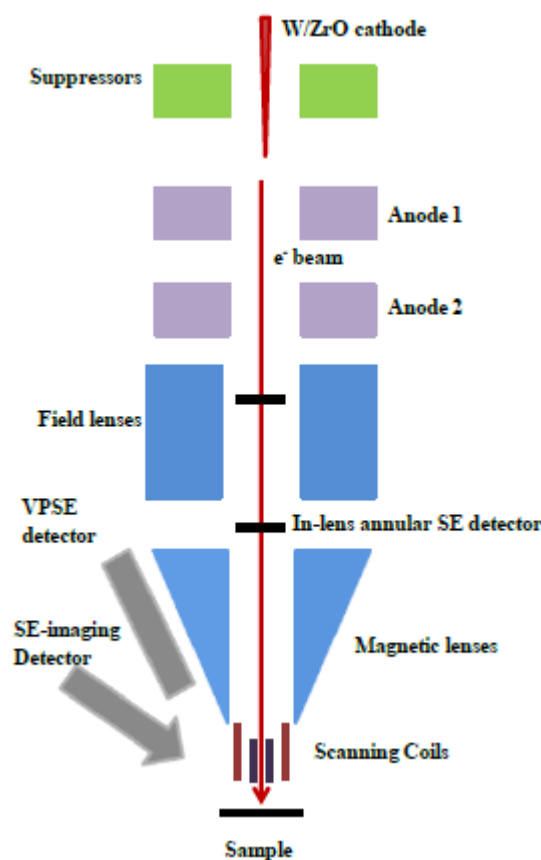

Figure 2.3.3: Schematic for illustration of Field Emission Scanning Electron Microscopy

2.2.3 Transmission Electron Microscopy (TEM)

The Transmission Electron Microscopy is a microscopy technique in which a beam of electrons is transmitted through the sample to produce an image. Compared to light microscope TEM produces high-resolution images as it uses electron beams for imaging and their wavelength is much smaller than photons used in the light microscope. Thus it can be used to obtain images to an atomic level providing information about the morphology, structure, crystallization and also the strain in the

sample. TEM requires a very thin sample so that the electrons are transmitted through the sample; so generally, we use carbon-coated TEM grids which are semipermeable to electrons. In TEM, a high-speed electron beam emitted from the electron gun is focused to the ultra-thin sample and according to its transparency part of the beam is transmitted and focused to form the image (Figure 2.3.4). The image is then passed through the projector lens to enlarge them and then it strikes on the phosphor screen and the light is generated, which allows to see an image that human eye can see. The High-resolution transmission electron (TEM) microscopy was performed with JEM 220 fs jeol 200 KV.
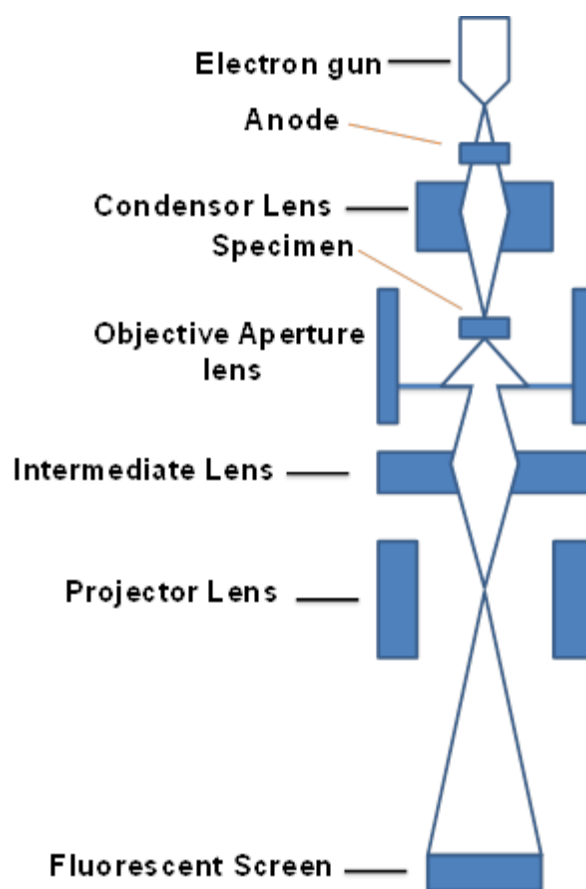

Figure 2.3.4: Schematic of Transmission electron microscopy

2.2.4 Energy Dispersive Analysis of X-rays (EDAX)

Energy Dispersive X-ray (EDX) analysis is a non-destructive technique used to comprehend the elements and their composition that are present in the sample by analysing the energy of X-ray emitted during the process. EDX systems are attached to Scanning Electron Microscopy (SEM) and Transmission Electron Microscopy (TEM) where the specimen of interest is identified by the imaging capability of the

microscope. Elemental mapping can be also done with the same systems which show the spatial distribution of elements in the sample.

The atoms in the sample are X-rayed with high energy electrons which kick out the electrons from the inner shells (Figure 2.3.5). Subsequently, electrons from the outer shell fall into the vacant place and result in a reduction in the potential energy of an electron and thus emit X-rays whose energy is atom dependent. The detection of this X-ray helps to distinguish the elements and its confirmation.
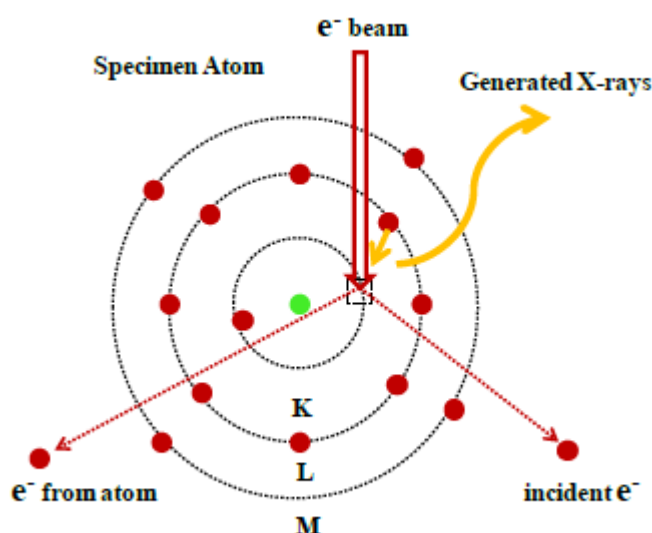

Figure 2.3.5: Schematic for illustration of the principle of EDX

2.3 Electrode and coin cell fabrication

The electrochemical measurements were done using 2016 coin cells. The electrode was made by using the sample, conducting carbon and CMC binder in 7:2:1 ratio.

Four different types of electrodes were made:

(a) Pristine material CaV_4O_9
(b) Pristine Si-NPs
(c) Composite of 20% Si-NPs and 80% CaV_4O_9
(d) Composite of 50% Si-NPs and 50% CaV_4O_9

The silicon nanoparticles and CVO were physically mixed using batch sonication with NMP as a solvent for uniform mixing. Later, the residual NMP was evaporated in the oven.

While preparing the coating for an electrode, sample conducting carbon and CNC binder was mixed with NMP using motor pistil to obtain a fine paste. Then, the paste was then evenly spread on copper foil and was dried for 2h at 70°C in an oven. The prepared coating was then punched into small wafers of diameter 1cm. The loading of the active material was about 0.65 to 4.75 mg cm^{-2}. The counter electrode used was Lithium metal; Celgard-2300 membrane was used as a separator and 1M LiPF$_6$ in 1:1 v/v EC/DMC as an electrolyte. The schematic of coil cell fabrication which was carried out inside a glove-box is shown in Figure 2.4.1.
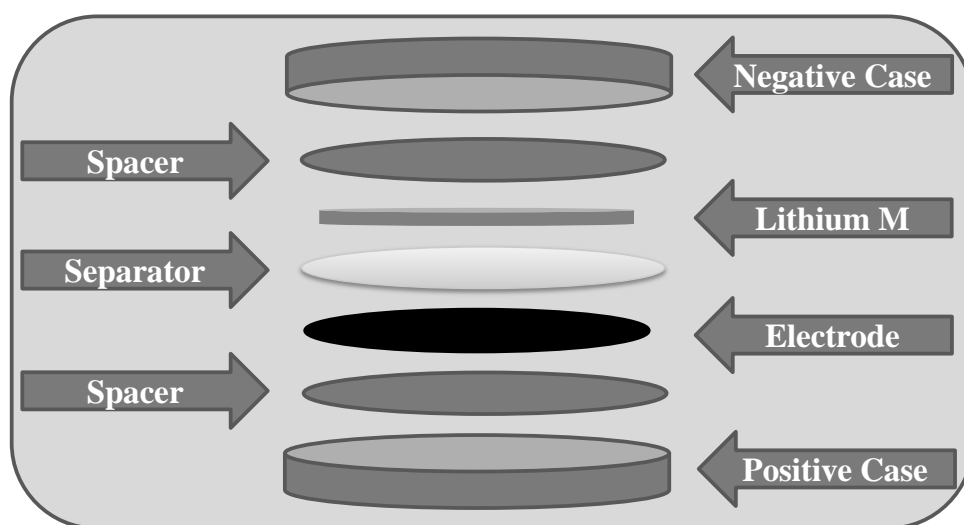

Figure 2.4.1: Coin cell assembly of electrode half-cell

2.4 Electrochemical characterization techniques

2.4.1 Cyclic voltammetry (CV)

The electrochemical properties associated with an electroactive surface area are studied using cyclic voltammetry (CV). The CV is a handy electrochemical technique that helps us understand the redox mechanism and transport properties of an electrochemical species of interest. These measurements are usually done using potentiostat where active redox species are scanned at different potentials. As electrode potential is varied as a function of time, the potentiostat measures the current through the circuit. Typically, a three-electrode system is used for CV measurements which include a working electrode, counter electrode and reference electrode. Here we have used a two electrode system in an electrochemical cell with lithium metal as the counter electrode. A potential range is applied across the working electrode and counter electrode, and resultant current is measured using an

ammeter (Figure 2.5.1). A voltammogram is a plot of current w.r.t applied voltage at a certain scan rate and starting from very low voltage like 0.01 V, with a scan rate of 0.1 mV s^{-1}, the current is measured. When the voltage reaches its maximum, the scanning is reversed and the negative current is measured. In a particular CV graph, there will be a cathodic peak and an anodic peak with hysteresis loop. CV measurements were done using PARSTAT MC automatic measurement system.
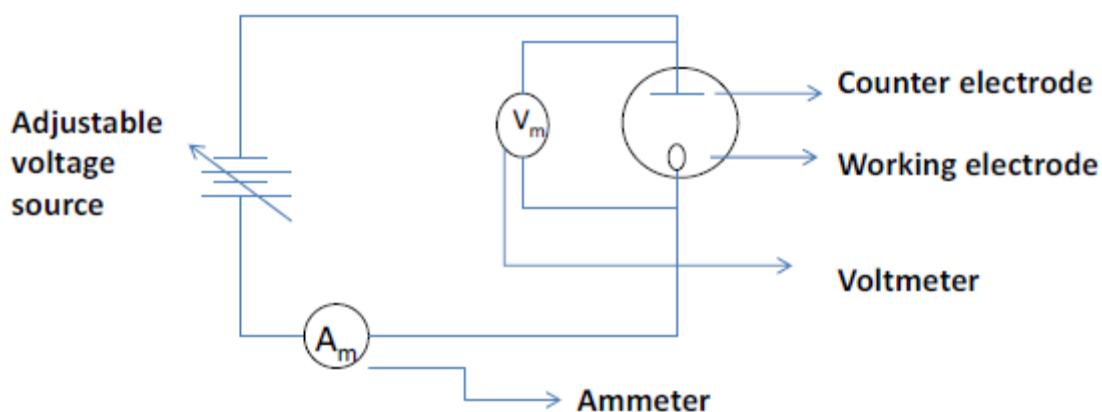

Figure 2.5.1: Circuit diagram of CV

2.4.2 Impedance

Impedance, a complex resistance with more than two components is a technique used to understand the battery kinetics. A Nyquist plot, i.e. the imaginary vs real resistance plot, is used to determine the kinetics of the species in the battery. The beginning of semi-circle describes the series resistance of the system that includes resistance from electrodes, circuit, cables, and contacts and reflects the electrolyte interaction at the anode surface. The total resistance of semi-circle is the electron or charge transfer resistance of the electrode. The region after the charge transfer resistance signifies the diffusion of ions from an electrolyte to electrode, also known as the mass transfer in the electrode.
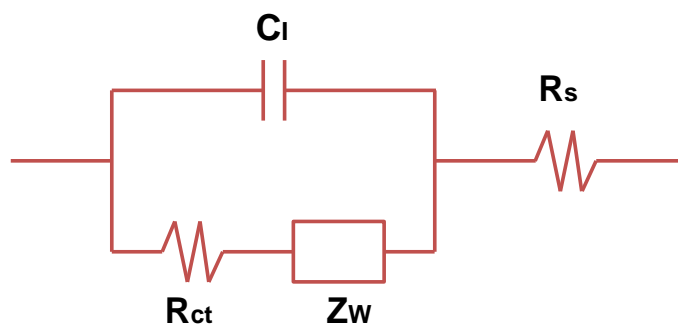
Figure 2.5.2: Impedance circuit

Equivalent circuit in place of electrode solution interface

Where, C_l – double layer capacitance

Z_W – faradic impedance includes the Warburg impedance

R_{ct} – the charge transfer

R_S – series resistance

2.4.3 Galvanostatic charge-discharge measurement

Galvanostatic charge-discharge gives information about specific capacity, specific energy and cycling stability where the current is controlled, and voltage is measured. A constant current is applied to the electrochemical cell and voltage is measured as a function of time. When the voltage reaches the maximum, the current is swiped reverse. This method is also known as chronopotentiometry, and it gives information about different parameters like capacitance, resistance and cyclability. In this method, a pulse of current is applied across the working electrode, and the resulting potential is measured across the reference electrode as a function of time.

Capacity is the total amount of electron charge transferred during the charging or discharging process.

Theoretical capacity gives the estimation of specific capacity that the battery can attend. Specific capacity can never exceed the theoretical capacity value.

$$C = \frac{n * F}{M.W.* 3.6}$$

Where, n- the number of Li-ions material can intake, F- Faraday's constant, i.e. 96500 C mol^{-1}, M.W. - molecular weight of active material g mol^{-1}.

The unit of theoretical capacity is mAh g^{-1}.

Specific charge/discharge capacity is given by,

$$Q = \frac{I * t}{m}$$

Where, I- current in mA, t- time in hours, m- the mass of active material in grams

The energy density of the battery is the amount of charge, i.e. Li-ions that can be stored in it. Energy density is given by,

$$E = Q * V$$
$$E = (It) * V$$

Where, E- energy density, Q- charge, V- voltage, I- current, t- time.

The unit of energy density is Whkg^{-1}.

A power density of the battery is the rate at which it can store or transport the charge.

It is given by,

$$P = \frac{E}{t}$$

Where, P- power, E- energy, t- time.

The unit of power density is W kg^{-1}.

Rate capability explains the ability of the active material to retain the capacity at different current densities. It is measured in a similar way as that of charge-discharge measurement by applying various current densities.

Cycling stability gives information about the durability electrochemical cell. It is a plot of specific capacity versus the number of cycles. The capacity degrades with time due to many reasons like side reactions taking place during cycling, the desolation of material in an electrolyte, degradation of the electrolyte with time, etc.

The coulombic efficiency provides information about side reactions that can take place during the charging/discharging process. It is the ratio of discharging capacity to the previous charging capacity. Coulombic efficiency less than 100% leads to an irreversible capacity loss in the electrochemical cell. This might happen due to dissolution if active material in the electrolyte during cycling or trapping of ions in nanopores of the material which cannot be taken out even if the similar potential is applied.

Solid Electrolyte Interphase (SEI) is an electronically insulating and ionically conducting porous layer that is formed when electrolyte gets reduced on the anode surface. In first discharge, electrolyte gets decompose to form Li-based compounds like Li_2CO_3, Li_2O, LiF and this contributes to irreversibly Li loss. This layer avoids the additional reduction of electrolyte during the charge-discharge process and also helps in proper diffusion of Li ions towards the material when it comes from the cathode with various forces.

The charge-discharge capacity measurements were carried out using NEWARE automatic coin cell testing system.

Chapter 3

Results and discussion

3.1 Structural characterization

3.1.1 PXRD

The powder X-ray diffraction (PXRD) data for structural analysis of the final product obtained is presented in Figure 2. It shows the pure phase tetragonal geometry of CaV_4O_9 without any impurity and is consistent with the JCPDS file no. 70-1325 *(a=8.32700, c=5.01300, S.G.: P4/n).* The (001) reflection plane at an angle of 17.5° is the characteristic peak of a layered structure, indicating the stable phase of CaV_4O_9 consistent with the FESEM images.
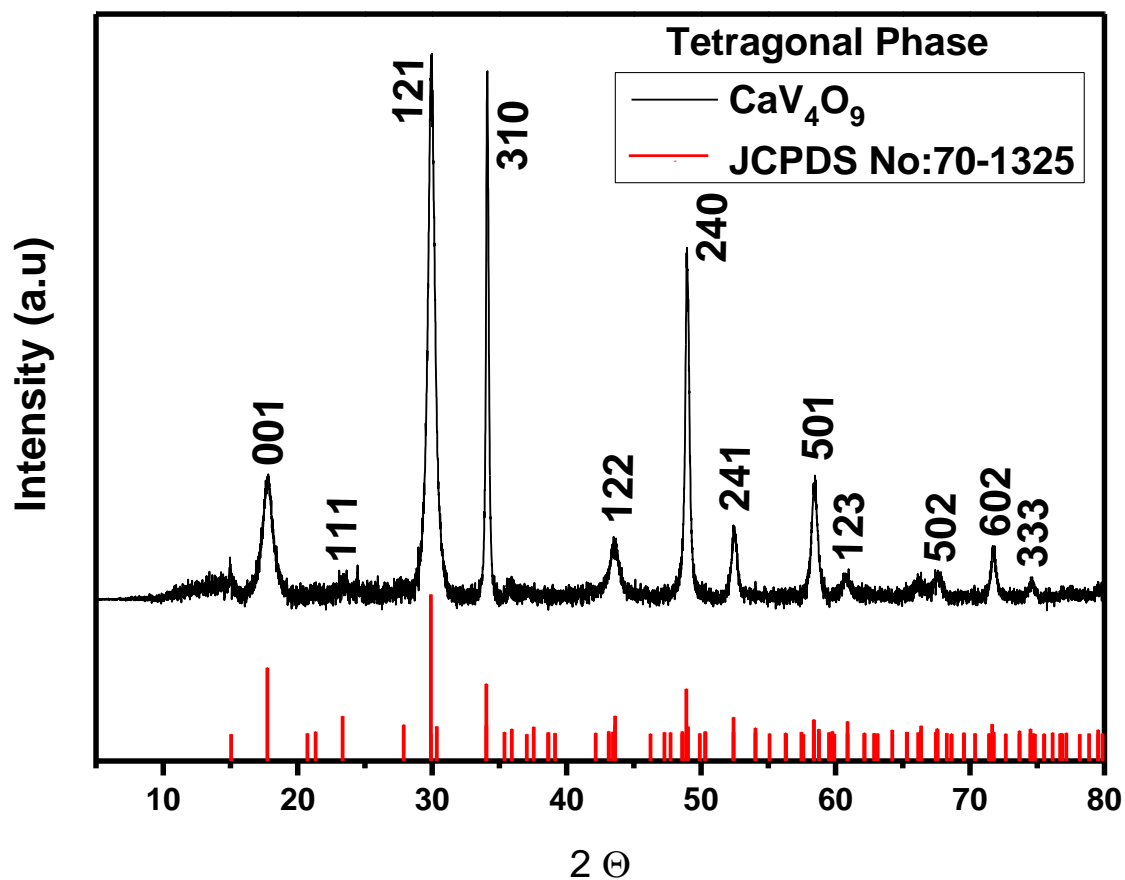

Figure 3.1: XRD pattern of CaV_4O_9

3.1.2 FESEM

The morphological study of the prepared samples is done using FESEM which is shown in Figure 2. The images of CaV4O9 confirm the microflower morphology formed by the assembly of several thin nanosheets. The size of the microflower is in the range of 1-3 µm. The EDAX mapping confirmed the presence of elements like calcium, vanadium and oxygen and their even distribution throughout the morphology (Figure 3.2 (d)).
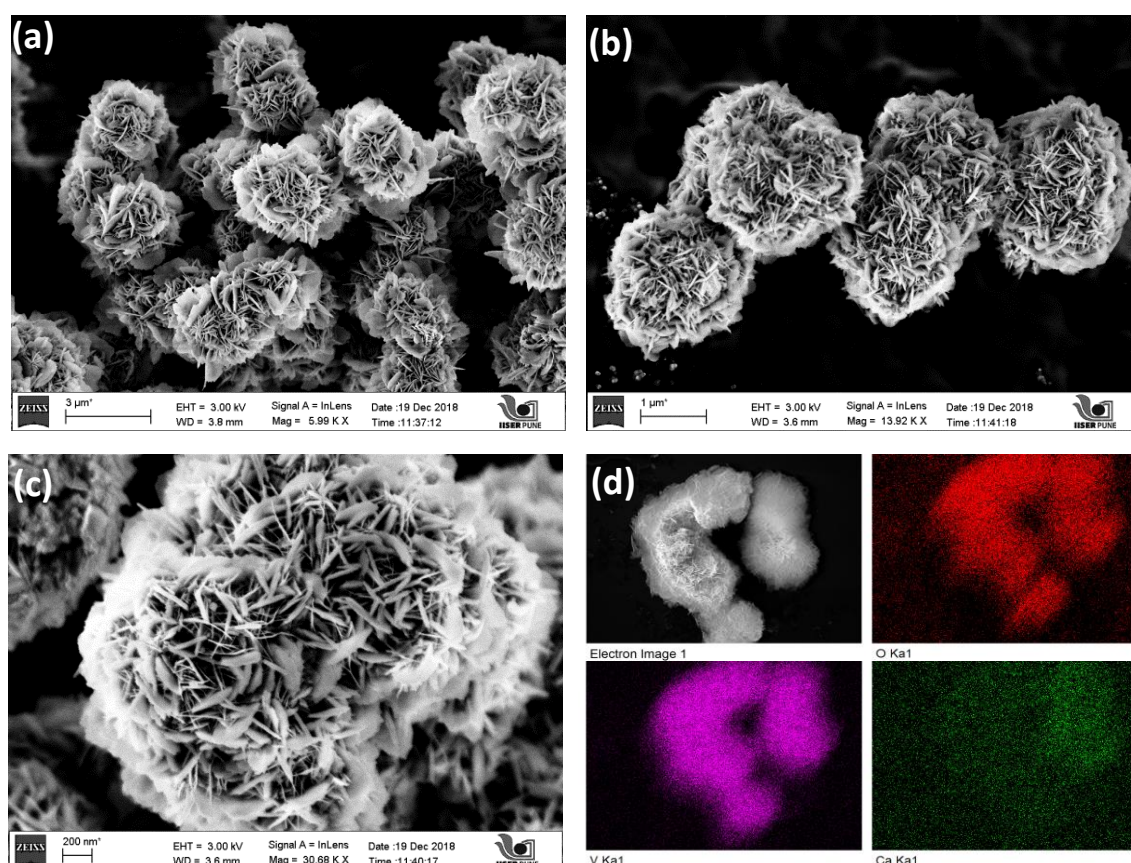

Figure 3.2: FESEM images and EDS mapping of CaV$_4$O$_9$

3.1.3 TEM and EDAX

The high-resolution TEM data of pristine CVO is presented in Figure 3.3.   The images show compact and solid morphology of microflower. The inter-planar spacing of 0.25 nm is seen in the image which corresponds to (310) plane of CVO. The selected area electron diffraction (SAED) arrangement reveals the single-crystalline characteristic of ultra-thin nanosheets, and the EDAX result shows that the Ca/V ratio of the sample obtained is 0.82/4.
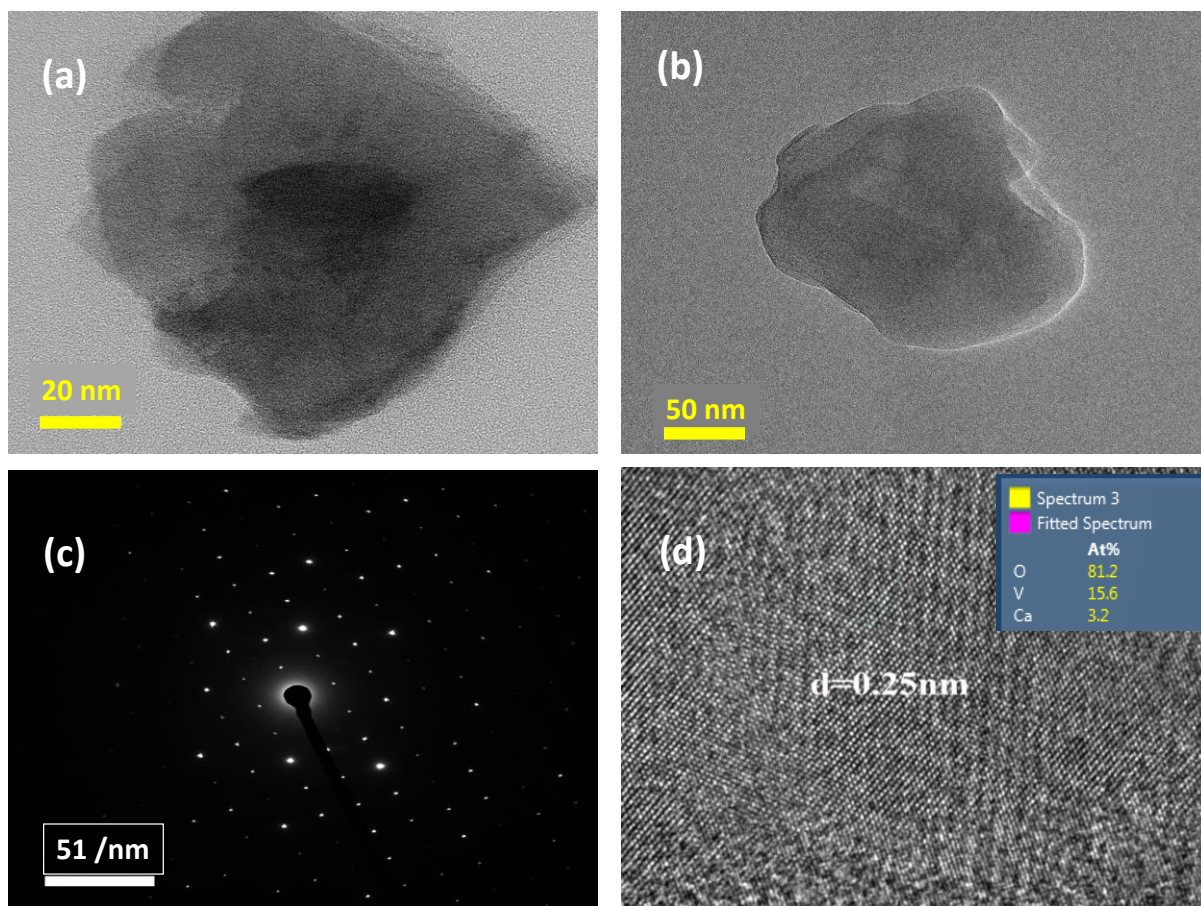
21

Figure 3.3: TEM images and a table showing the elemental composition

3.2 Electrochemical characterization

Battery capacity measurements were done using a Lithium coin cell battery.

Case (I): **Pristine CaV_4O_9:** During charge-discharge measurements, the cell was run at 100 mA g^{-1}, initial discharge capacity which is also called as the irreversible capacity of 1507.406 mAh g^{-1} was observed with reversible capacity of 800 mAh g^{-1} (Figure 3.4.1 a). The cycling stability with an average specific capacity of 700 mAh g^{-1} was observed for around 140 cycles (Figure 3.4.1 b). Rate performance was measured at different densities starting from 500 mA g^{-1} to 3 A g^{-1}, and different specific capacity was observed. When the current density was reduced from 3 A g^{-1} to 200 mA g^{-1}, the initial capacity was maintained indicating excellent stability at higher current densities (Figure 3.4.1 c). The following data in Figure 3.4.1 shows the measurements of electrode half-cell made using a coin cell at a current rate of 100 mA g^{-1}.
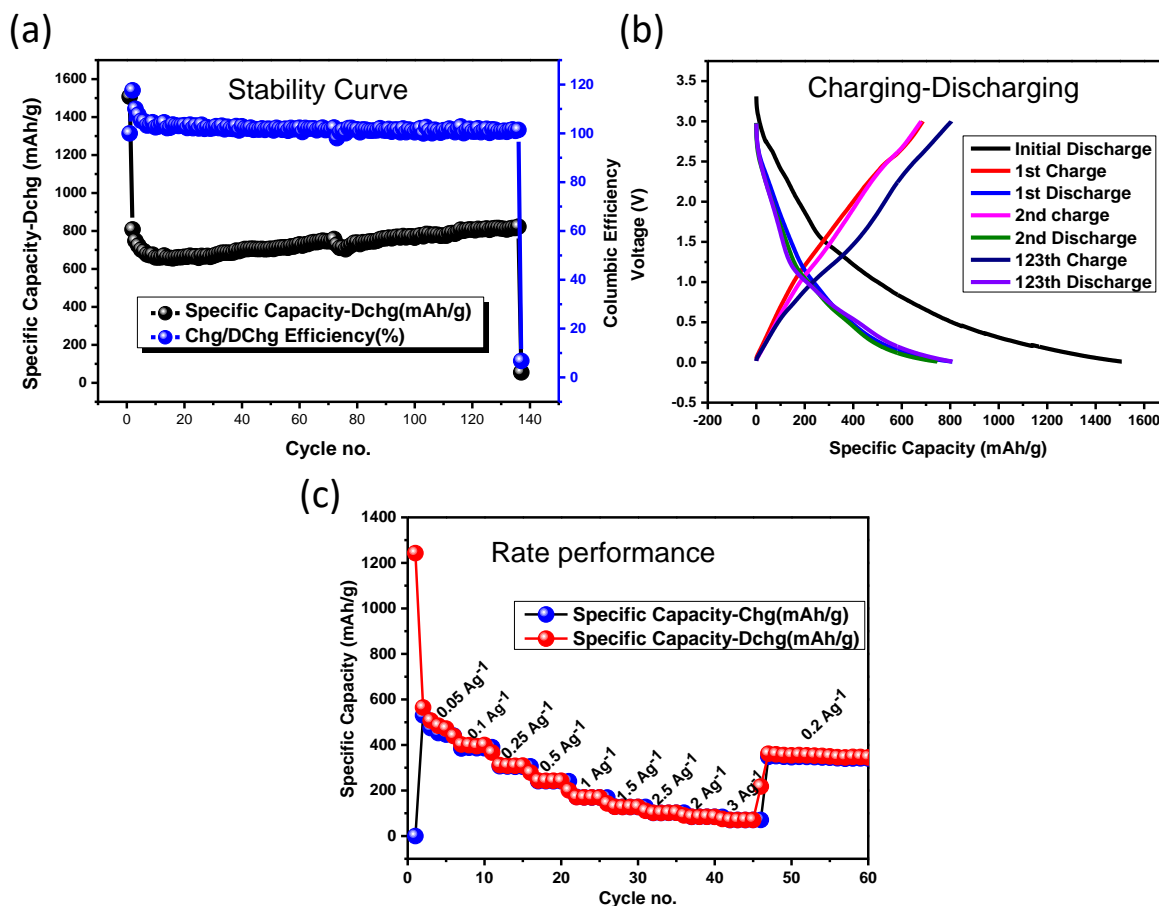
Figure 3.4.1: Electrochemical properties of CaV$_4$O$_9$ micro-flowers at 100 mA g^{-1}.

(a) Cyclic stability performance of CVO (b) The Charge-Discharge profile of CVO (c) Rate performance of CVO at altered current densities.

When the cell was measured at a current rate of 1 A g^{-1}, the initial discharge capacity of pristine CVO is 290 mAh g^{-1}, and it reached around 90 mAh g^{-1} after 100 cycles as shown in Figure 3.4.2 (c, d). The nature of CV in Figure 3.4.2 (a) at 0.1 V shows that this is intercalation type material for the anode. The multiple peaks in CV represent the side reactions that can take place during cycling and alloy formation of vanadium with lithium. As vanadium have multiple valence states it can undergo redox reactions at different potentials. The series resistance is negligible as shown in the impedance plot, and the charge transfer resistance is low compared to other oxide material with high mass transfer in the electrode(Figure 3.4.2 b).
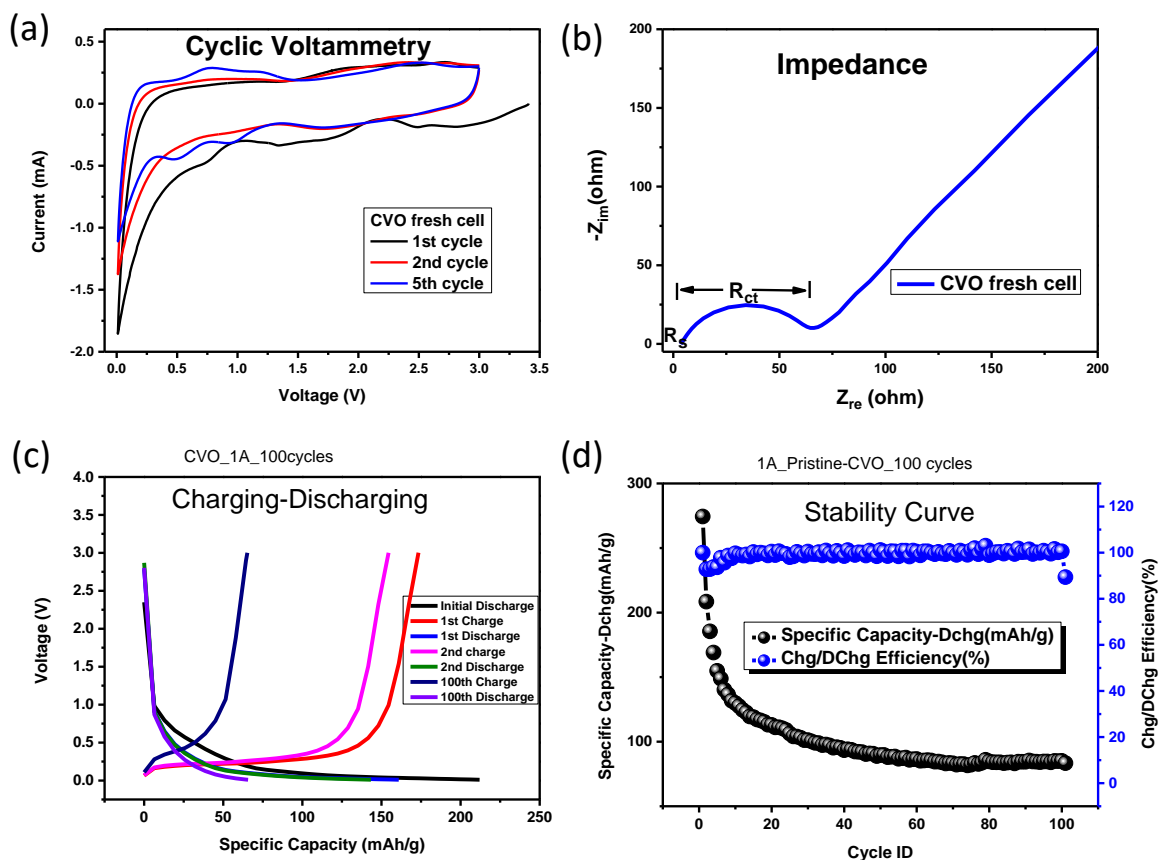
Figure 3.4.2: Electrochemical measurements of pristine CVO microflowers at 1 A g^{-1}.

(a) Cyclic voltammetry measurement (b) Impedance measurement (c) Charge-discharge curve and (d) Stability curve carried out on pristine CVO microflowers.

Case (II): **Pristine Si-NPs:** In charge-discharge measurements, a very high initial discharge capacity of 2938.13 mAh g^{-1} was observed and but within 50 cycles the capacity has gone below 50 mAh g^{-1} due to the volume expansion of silicon. From impedance measurements (Figure 3.4.3 b), we can see that pristine Si-NPs anode possesses very low series resistance due to the smaller size of nanoparticles which facilitates quick electrolyte percolation into the electrode surface. The charge transfer resistance of pristine Si NPs anode is very high as the nanoparticles are non-conducting in nature despite their smaller size.

The typical CV curves for anode were obtained by scanning between 0.01 – 3 V with a scan rate of 0.1 mV s^{-1} and the data is shown in Figure 3.4.2. The broad peak at 1.0 V in Si-NPs anode, a cathodic scan is due to the SEI formation due to the electrolyte decomposition at the electrode surface. The

24

peak observed at 0.21 V in the cathodic part indicates the Li-Si alloy formation during lithiation. During the anodic scan, the peaks noted at 0.3 V and 0.48 V corresponds to the de-lithiation of Li-Si alloys. It is also observed that the peak intensity in the Si-NPs anode case reduces during cycling due to the cracking of anode.
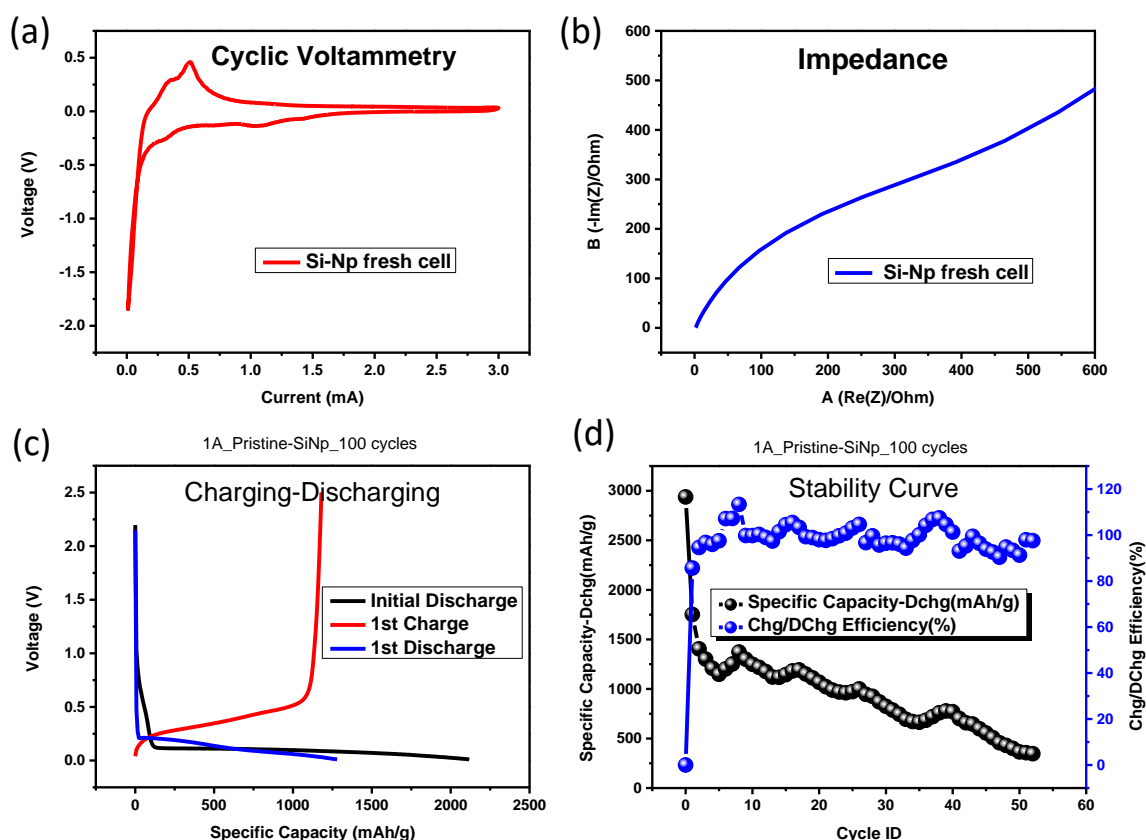

Figure 3.4.3: Electrochemical measurements of pristine Si-NPs carried out at 1 A g^{-1}.

(a) Cyclic voltammetry measurement (b) Impedance measurement (c) Charge-discharge curve and (d) Stability curve performed on pristine Si-NPs.

Case (III): **Composite of 80% CaV$_4$O$_9$ and 20% Si-NPs:** During charge-discharge measurements, the initial discharge capacity of 1232.14 mAh g^{-1} was observed, and it reduced to 450 mAh g^{-1} at 1 A within 100 cycles. Unlike pristine silicon case, this composite is stable, and the specific capacity is higher than pristine CVO after 100 cycles. Figure 3.4.4 shows the stability and charge-discharge curve of this composite.
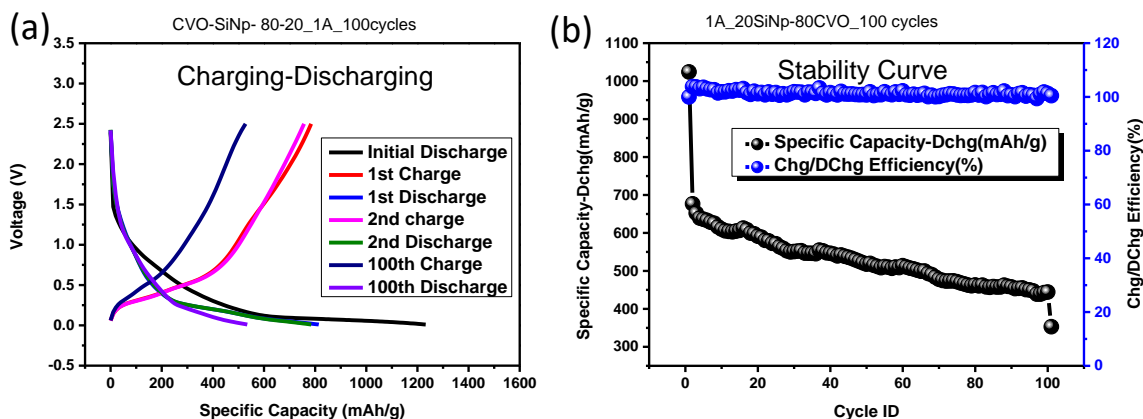
Figure 3.4.4: Electrochemical measurements of CVO-SiNPs (80-20) composite at 1 A g^{-1}.

(a) Charge-Discharge measurements (b) Stability curve measurements performed on CVO-Si-Np (80-20) composite.

Case (IV): **Composite of 50% CaV$_4$O$_9$ and 50% Si-NPs:** While the charge-discharge measurements carried out at 1 A, the initial discharge capacity of 1760.03 mAh g^{-1} was observed with stable reversible capacity of 800 mAh g^{-1} for 100 cycles. The stability is remarkable unlike pristine silicon which decreases in 50 cycles, and the specific capacity value is 6-7 times higher than pristine CVO.
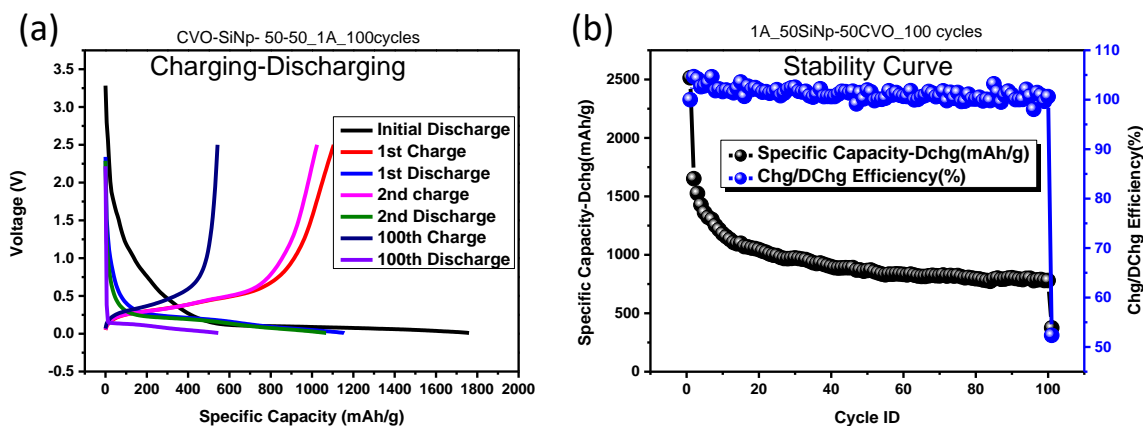

Figure 3.4.5: Electrochemical measurements of CVO-SiNPs (50-50) composite at 1 A g^{-1}.

(a) Charge-Discharge measurements (b) Stability curve measurements performed on CVO-Si-Np (50-50) composite.
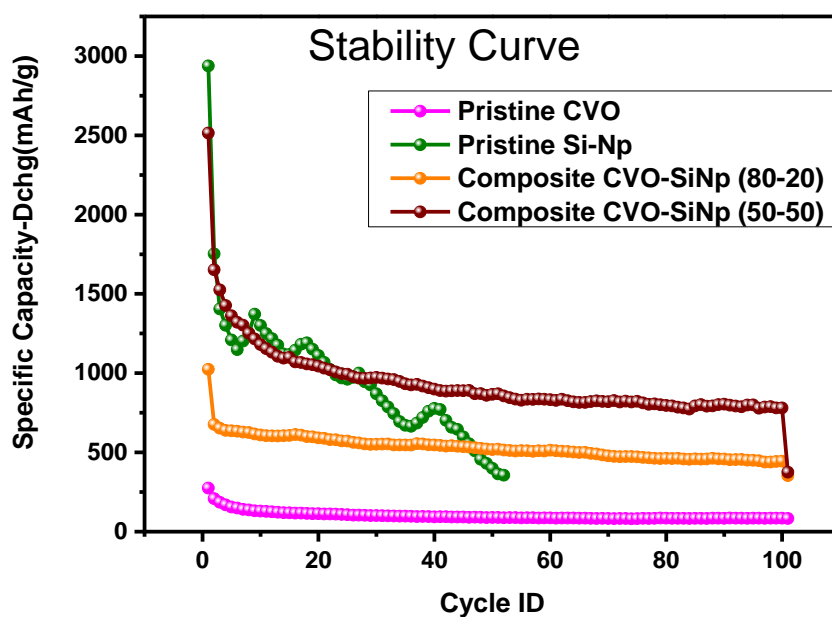
Figure 3.4.6: Comparison of stability plots of CVO, Si-NPs and their composites at 1 A g^{-1}.

Figure 3.4.6 compares the stability curve of pristine samples and their composites. The initial discharge capacity of Si-NPs anode is very high compared to all other samples but, within 50 cycles it fades to 50 mAh g^{-1}. This happens due to the volume expansion of about 300% in the pristine silicon-based anode. On the other hand, pristine CVO shows a stable capacity of around 100 mAh g^{-1} for 100 cycles. When composites of Si-NPs and CVO were prepared, their capacity is pretty much higher and stable than the pristine ones. In the case of 80-20 CVO-Si-NPs, the capacity increased by 4-folds, and in the case of 50-50 CVO-Si-NPs, the capacity increased by 7-folds. In the composite materials, the volume expansion of Si-NPs is taken care of by the robust and dense morphology of CVO.

Chapter 4

Summary and future prospects

To summarize, a hydrothermal method was used to synthesize the CaV_4O_9 microflowers and phase pure tetragonal structure was obtained. The physical and chemical characterizations of CVO were done using various techniques like XRD, FESEM, and TEM. The composites of CVO and Si-NPs in different proportions were also made. The Galvanostatic charge-discharge measurements were performed for CVO, Si-NPs, CVO-Si-NPs (80-20) and CVO-Si-NPs (50-50) for studying their stability and specific capacity. Electrochemical characterizations such as CV, impedance measurements, and rate performance were carried out on these four samples. After 100 cycles at 1A, pristine CVO shows the stable capacity of 90 mAh g^{-1} whereas within 50 cycles pristine Si-NPs battery fades its capacity and the battery dies with very high initial discharge capacity. This is due to volume expansion that takes place during cycling.

The composites of CVO with Si-NPs show higher specific capacity with good cycling stability. With the composite of 80-20 CVO-Si-NPs, when the battery was run at a high current rate of 1 A, the specific capacity is 450 mAh g^{-1}. And in case of 50-50 CVO-Si-NPs composite, a very high specific capacity of 800 mAh g^{-1} was achieved. This is attributed to the robust stability of CVO where it acts as a buffer matrix to absorb the volume expansion occurring in Si-NPs during lithiation and preventing the pulverization. Although it delivers a low specific capacity at high rates but it acts as a support for Si-NPs.

Future studies:

- Exploring alkaline earth metal vanadates containing Strontium, Magnesium, etc. for anode materials to enhance battery performance.
- Magnesium-based vanadates can also be explored as cathode material in LIBs.
- To improve the overall performance of LIB technology and introduce various elements in battery technology.

References

1.   Xu, X. *et al.* Alkaline earth metal vanadates as sodium-ion battery anodes. *Nat. Commun.* **8,** 1–10 (2017).

2.   Power vs Energy.png (500×348). Available at: http://www.seas.ucla.edu/~pilon/images/supercapacitors/Power vs Energy.png. (Accessed: 11th March 2019)

3.   Jecker, J. & Landy, D. Liking a Person as a Function of Doing Him a Favour. *Hum. Relations* **22,** 371–378 (1969).

4.   Focaccia, M. & Simili, R. Luigi Galvani, Physician, Surgeon, Physicist: From Animal Electricity to Electro-Physiology. in *Brain, Mind and Medicine: Essays in Eighteenth-Century Neuroscience* 145–158 (Springer US, 2007). doi:10.1007/978-0-387-70967-3_11

5.   Salles, P., Gauche, R. & Virmond, P. A Qualitative Model of Daniell Cell for Chemical Education. in 870–872 (2004). doi:10.1007/978-3-540-30139-4_103

6.   Ogude, A. N. & Bradley, J. D. Ionic Conduction and Electrical Neutrality in Operating Electrochemical Cells: Pre-College and College Student Interpretations. *J. Chem. Educ.* **71,** 29 (1994).

7.   Green, A. The characteristics of the nickel-cadmium battery for energy storage. *Power Eng. J.* **13,** 117–121 (1999).

8.   Putois, F. Market for nickel-cadmium batteries. *J. Power Sources* **57,** 67–70 (1995).

9.   Whittingham, M. S. Lithium Batteries and Cathode Materials. (2004). doi:10.1021/cr020731c

10.   Akinlo, A. E. Energy consumption and economic growth: Evidence from 11 Sub-Sahara African countries. *Energy Econ.* **30,** 2391–2400 (2008).

11.   Křepelková, M. *Evolution of batteries: From experiments to everyday usage.*

12.   Lithium-ion-Battery-Explanation.jpg (700×244). Available at: https://i0.wp.com/blog.ravpower.com/wp-content/uploads/2017/05/Lithium-ion-Battery-Explanation.jpg. (Accessed: 5th March 2019)

13.   Goodenough, J. B. & Park, K.-S. The Li-Ion Rechargeable Battery: A Perspective. *J. Am. Chem. Soc.* **135,** 1167–1176 (2013).

14.   Attidekou, P. S. *et al.* A study of 40 Ah lithium ion batteries at zero percent state of charge as a function of temperature. *J. Power Sources* **269,** 694–703 (2014).

15. Tarascon, J.-M. & Armand, M. Issues and challenges facing rechargeable lithium batteries. *Nature* **414,** 359–367 (2001).

16. Miroshnikov, M. *et al.* Power from nature: designing green battery materials from electroactive quinone derivatives and organic polymers. *J. Mater. Chem. A* **4,** 12370–12386 (2016).

17. McDowell, M. T., Lee, S. W., Nix, W. D. & Cui, Y. 25th Anniversary Article: Understanding the Lithiation of Silicon and Other Alloying Anodes for Lithium-Ion Batteries. *Adv. Mater.* **25,** 4966–4985 (2013).

18. Xu, X. *et al.* Realizing stable lithium and sodium storage with high areal capacity using novel nanosheet-assembled compact CaV4O9microflowers. *Nano Energy* **50,** 606–614 (2018).

19. Levi, M. D. & Aurbach, D. Diffusion Coefficients of Lithium Ions during Intercalation into Graphite Derived from the Simultaneous Measurements and Modeling of Electrochemical Impedance and Potentiostatic Intermittent Titration Characteristics of Thin Graphite Electrodes. *J. Phys. Chem. B* **101,** 4641–4647 (1997).

20. Schipper, F. & Aurbach, D. A brief review: Past, present and future of lithium ion batteries. *Russ. J. Electrochem.* **52,** 1095–1121 (2016).

21. Andre, D., Hain, H., Lamp, P., Maglia, F. & Stiaszny, B. Future high-energy density anode materials from an automotive application perspective. *J. Mater. Chem. A* **5,** 17174–17198 (2017).

22. Zhang, W.-J. A review of the electrochemical performance of alloy anodes for lithium-ion batteries. *J. Power Sources* **196,** 13–24 (2011).

23. Oumellal, Y., Rougier, A., Nazri, G. A., Tarascon, J.-M. & Aymard, L. Metal hydrides for lithium-ion batteries. *Nat. Mater.* **7,** 916–921 (2008).

24. Chae, J. H., Ng, K. C. & Chen, G. Z. Nanostructured materials for the construction of asymmetrical supercapacitors. *Proc. Inst. Mech. Eng. Part A J. Power Energy* **224,** 479–503 (2010).

25. Wang, R. *et al.* Effect of Different Binders on the Electrochemical Performance of Metal Oxide Anode for Lithium-Ion Batteries. *Nanoscale Res. Lett.* **12,** 575 (2017).

26. Ponrouch, A., Marchante, E., Courty, M., Tarascon, J.-M. & Palacín, M. R. In search of an optimized electrolyte for Na-ion batteries. *Energy Environ. Sci.* **5,** 8572 (2012).

27. Nanotechnology, X. Y.-J. of S. S. and & 2012, undefined. Controlled synthesis of calcium sulfate and calcium vanadate nanostructures. *jstage.jst.go.jp*

28. Pei, L. *et al.* Formation process of calcium vanadate nanorods and their

electrochemical sensing properties. *cambridge.org*

29. Cromer, C. E. Preparation and characterization of vanadium oxides on carbon fiber paper as electrodes for pseudocapacitors. (2013). doi:10.1016/j.bone.2008.01.030

30. Muldoon, J., Bucur, C. B. & Gregory, T. Quest for Nonaqueous Multivalent Secondary Batteries: Magnesium and Beyond. *Chem. Rev.* **114,** 11683–11720 (2014).

31. Kasavajjula, U., Wang, C. & Appleby, A. J. Nano- and bulk-silicon-based insertion anodes for lithium-ion secondary cells. *J. Power Sources* **163,** 1003–1039 (2007).

32. Zhang, W.-J. Lithium insertion/extraction mechanism in alloy anodes for lithium-ion batteries. *J. Power Sources* **196,** 877–885 (2011).

33. Park, M.-H. *et al.* Silicon Nanotube Battery Anodes. *Nano Lett.* **9,** 3844–3847 (2009).

34. Yang, Y. *et al.* New Nanostructured Li $_2$ S/Silicon Rechargeable Battery with High Specific Energy. *Nano Lett.* **10,** 1486–1491 (2010).

35. Thakur, M. *et al.* Freestanding Macroporous Silicon and Pyrolyzed Polyacrylonitrile As a Composite Anode for Lithium Ion Batteries. *Chem. Mater.* **24,** 2998–3003 (2012).